

Bilayered Hybrid Perovskite Ferroelectric with Giant Two-Photon Absorption

Lina Li,[†] Xiaoying Shang,[‡] Sasa Wang,[†] Ningning Dong,[§] Chengmin Ji,[†] Xueyuan Chen,^{*,†,ID}
Sangen Zhao,^{†,ID} Jun Wang,^{§,ID} Zhihua Sun,^{*,†} Maochun Hong,^{†,ID} and Junhua Luo^{*,†,ID}

[†]State Key Laboratory of Structural Chemistry, Fujian Institute of Research on the Structure of Matter, Chinese Academy of Sciences, Fuzhou, Fujian 350002, China

[‡]CAS Key Laboratory of Design and Assembly of Functional Nanostructures, and Fujian Key Laboratory of Nanomaterials, Fujian Institute of Research on the Structure of Matter, Chinese Academy of Sciences, Fuzhou, Fujian 350002, China

[§]Key Laboratory of Materials for High-Power Laser, Shanghai Institute of Optics and Fine Mechanics, Chinese Academy of Sciences, Shanghai 201800, China

S Supporting Information

ABSTRACT: Perovskite ferroelectrics with prominent nonlinear optical absorption have attracted great attention in the field of photonics. However, they are traditionally dominated by inorganic oxides and exhibit relatively small nonlinear optical absorption coefficients, which hinder their further applications. Herein, we report a new organic–inorganic hybrid bilayered perovskite ferroelectric, $(\text{C}_4\text{H}_9\text{NH}_3)_2(\text{NH}_2\text{CHNH}_2)\text{Pb}_2\text{Br}_7$ (**1**), showing an above-room-temperature Curie temperature (~ 322 K) and notable spontaneous polarization ($\sim 3.8 \mu\text{C cm}^{-2}$). Significantly, the unique quantum-well structure of **1** results in intriguing two-photon absorption properties with a giant nonlinear optical absorption coefficient as high as $5.76 \times 10^3 \text{ cm GW}^{-1}$, which is almost two-orders of magnitude larger than those of mostly traditional all-inorganic perovskite ferroelectrics. To our best knowledge, **1** is the first example of hybrid ferroelectrics with giant two-photon absorption coefficient. The mechanisms for ferroelectric and two-photon absorption are revealed. This work will shed light on the design of new ferroelectrics with two-photon absorption and promote their potentials in the photonic application.

been realized by Zeng's group.⁵ In this aspect, two-photon absorption behaviors of perovskite ferroelectrics have been widely studied, such as BaTiO_3 ,⁶ Ce:BaTiO_3 ,⁶ $\text{Bi}_{3.15}\text{Nd}_{0.85}\text{Ti}_3\text{O}_{12}$,⁷ $\text{Pb}_{0.7}\text{La}_{0.3}\text{TiO}_3$,⁸ $\text{SrBiTa}_2\text{O}_9$,⁹ and $\text{Pb}_{0.95}\text{La}_{0.05}\text{Zr}_{0.53}\text{Ti}_{0.47}\text{O}_3$.¹⁰ However, the majority of such perovskite ferroelectrics are all-inorganic and exhibit relatively small two-photon absorption coefficients, such as 51.7 cm GW^{-1} for BaTiO_3 , 59.3 cm GW^{-1} for Ce:BaTiO_3 , and 115 cm GW^{-1} for $\text{Bi}_{3.15}\text{Nd}_{0.85}\text{Ti}_3\text{O}_{12}$. This disadvantage becomes the potential bottleneck for their further device application.¹¹ In this context, it is highly urgent to develop new classes of ferroelectric candidates with large two-photon absorption coefficients.

Two-dimensional (2D) hybrid perovskites display great flexibility to accommodate a variety of organic ammonium cations, which enables the large freedom of molecular motions. From a structural perspective, such dynamic components are the key elements to create ferroelectricity, as exemplified by some recently reported 2D perovskite hybrid ferroelectrics, such as $(\text{benzylammonium})_2\text{PbCl}_4$ ¹² and $(\text{cyclohexylammonium})_2\text{PbBr}_4$.¹³ These 2D perovskites represent an interesting research direction in the development of ferroelectrics and are attracting increasing attention.¹⁴ Moreover, hybrid perovskites combine distinct properties of organic and inorganic components within a single-molecule composite,¹⁵ and thus show rich physical properties, such as two-photon absorption.¹⁶ Particularly, for 2D perovskites, their unique quantum-well structures favor the confinement of charge-carriers in inorganic layers and thus enhance light-matter interactions. This feature is considered to be quite suitable to generate strong two-photon absorption effects.¹⁷ For instance, a giant two-photon absorption coefficient has been obtained in a 2D layered perovskite of $[\text{C}_6\text{H}_5(\text{CH}_2)_2\text{NH}_3]_2\text{PbI}_4$.^{17b}

Inspired by the above-mentioned results, we designed and synthesized a new 2D hybrid perovskite, $(\text{BA})(\text{FA})\text{Pb}_2\text{Br}_7$ (**1**, BA = *n*-butylammonium and FA = formamidinium). **1** shows an above-room-temperature Curie temperature (~ 322 K), and notable spontaneous polarization ($\sim 3.8 \mu\text{C cm}^{-2}$). Strikingly, **1**

For ferroelectric materials, the combination of ferroelectricity with other physical properties makes them fascinating candidates for next-generation optoelectronic devices.¹ This unique feature leads to some newly conceptual topics in condensed-matter science, such as photoferroelectrics.² In photoferroelectrics, the strong inversion symmetry breaking inducing spontaneous electric polarization promotes the desirable separation of photoexcited carriers, which readily benefits their optoelectronic and photovoltaic applications.³ Recently, light–matter interactions in the ferroelectric materials have emerged as one of the intriguing characteristics.⁴ Among them, prominent two-photon absorption properties not only promise nonlinear photonic application but also fulfill the essential requirements of high-performance vis-IR dual-modal light harvesting optoelectronic device. For example, high-performance IR (two-photon) harvest and photodetection has

Received: April 15, 2018

Published: May 17, 2018



exhibits a giant two-photon absorption coefficient up to $5.76 \times 10^3 \text{ cm GW}^{-1}$, which is nearly two-orders of magnitude larger than those of the traditional all-inorganic perovskite ferroelectrics. Single crystals of **1** were obtained from the solution of concentrated hydrobromic acid containing stoichiometric amounts of $\text{Pb}(\text{COOH})_2 \cdot 3\text{H}_2\text{O}$, formamidinium acetate and *n*-butylamine. The measured powder XRD pattern matches well with that simulated based on single-crystal structure (Figure S1), confirming the pure phase of **1**. This perovskite is environmentally stable at ambient condition and exhibits a high thermal stability up to 252°C (Figure S2). Single-crystal X-ray diffraction reveals that **1** crystallizes in a polar space group of $Cmc2_1$ at room temperature (Table S1), and adopts a distinct bilayered perovskite. As shown in Figure 1a, the crystal

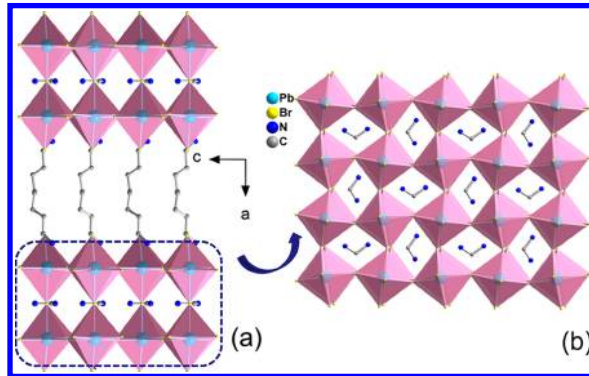


Figure 1. (a) Bilayered perovskite structure of **1**. (b) $[\text{Pb}_2\text{Br}_7]_\infty$ bilayered framework.

structure of **1** is composed of $[\text{Pb}_2\text{Br}_7]_\infty$ bilayers, which stack along the *a*-axis with BA^+ cations residing in the interlayer space to serve as interlayer connectors (via $\text{N}-\text{H}\cdots\text{Br}$ hydrogen bonds, Figure S2 and Table S2) and to maintain charge balance. Resembling the 3D framework of FAPbBr_3 , the FA^+ cations in **1** are confined in the central cavities assembled by PbBr_6 corner-sharing octahedra. In **1**, PbBr_6 octahedra displays a small-angle distortion as compared to the ideal octahedra, as disclosed by the $\text{Br}-\text{Pb}-\text{Br}$ bond angles (Table S3). Besides, the $\text{Pb}-\text{Br}-\text{Pb}$ bond angle (163.5°) deviates from the ideal value of 180° by about 27° (Figure S3), leading to the formation of distortion quadrangle with different diagonals (5.1 and 6.8 Å). Finally, distorted PbBr_6 octahedra link with their neighbors to form inorganic layer along *ab*-plane (Figure 1b). These inorganic layers are tightly connected to each other via the bridged Br atoms to generate $[\text{Pb}_2\text{Br}_7]_\infty$ bilayers. Such bilayers framework resembles those of other reported hybrid perovskites, such as $(\text{RCH}_2\text{NH}_3)_2(\text{CH}_3\text{NH}_3)_{n-1}\text{Sn}_3\text{I}_{3n+1}$ ¹⁸ and $(\text{C}_4\text{H}_9\text{NH}_2\text{NH}_3)(\text{CH}_3\text{NH}_3)_n\text{Pb}_3\text{I}_{3n+1}$,¹⁹ and all-inorganic perovskites (e.g., $\text{Ca}_3\text{Ti}_2\text{O}_7$ and $\text{Sn}_{n+1}\text{Ti}_n\text{O}_{2n+1}$).²⁰ It needs to be emphasized that the alternative stacking of organic and inorganic components in this bilayered perovskite can be regarded as a quantum-well structure with inorganic layers as the well and organic layers as the barrier. Because of the unique quantum and dielectric confinements in quantum-well structure, the carriers can be strongly confined in the inorganic layer to enhance light–matter interaction. Consequently, a prominent two-photon absorption property could be expected for **1**.^{17a}

Symmetry-breaking phase transitions are indispensable for the most of ferroelectrics. Differential scanning calorimetry (DSC) traces of **1** show a pair of thermal peaks at $322/318\text{ K}$ in

the heating and cooling modes, implying a reversible phase transition (Figure 2a). Moreover, large dielectric anomalies

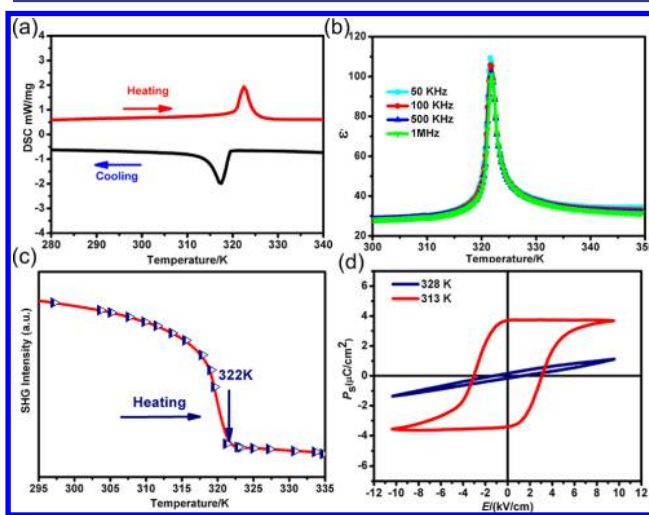


Figure 2. Ferroelectric and related properties of **1**. (a) DSC curves. (b) Temperature-dependent dielectric constants measured along the *c*-axis. (c) Temperature dependence of SHG signals, revealing a symmetry-breaking phase transition. (d) *P*–*E* hysteresis loops measured along the *c*-axis via double-wave method at different temperatures.

were also observed around 322 K for single crystal along the *c* axis, as shown in Figure 2b. The dielectric response at 500 Hz fits well with the Curie–Weiss law, $\epsilon' = C_{\text{para}}/(T - T_0)$ ($T > T_c$) or $C_{\text{ferro}}/(T_0' - T)$ ($T < T_c$), where C_{para} and C_{ferro} are the Curie constants, and T_0 and T_0' are the Curie–Weiss temperatures for the paraelectric and ferroelectric phases, respectively. The $C_{\text{para}}/C_{\text{ferro}}$ ratio of 2.1 agrees well with the theoretical value expected for a second-order ferroelectric phase transition (Figure S4).

Furthermore, variable temperature second harmonic generation (SHG) effects were performed to confirm that **1** undergoes a ferroelectric phase transition from a non-centrosymmetric to a centrosymmetric state. As shown in Figure 2c, the SHG activity of **1** changes obviously at around 322 K. The evident change of SHG indicates the occurrence of symmetry breaking in **1**, which is one of the characteristics for ferroelectric.²¹ To further verify the ferroelectric phase transition, *P*–*E* hysteresis loops were measured. As shown in Figure 2d, the linear curve of *P*–*E* dependence at 328 K indicates its paraelectric property. Below T_c , the characteristic ferroelectric loop was acquired via double-wave method.²² The hysteresis loop at 313 K affords the P_s value of $\sim 3.8 \mu\text{C}/\text{cm}^2$, which is close to that calculated from the point charge model (Supporting Information, Figure S8). This value is larger than those found for other organic–inorganic hybrids, such as $\text{N}(\text{CH}_3)_4\text{CdBr}_3$ ($\sim 0.12 \mu\text{C}/\text{cm}^2$),²³ $(\text{C}_5\text{H}_9\text{NH}_3)\text{CdCl}_3$ ($\sim 1.7 \mu\text{C}/\text{cm}^2$),²⁴ and comparable to those of (pyrrolidinium) MnCl_3 ($\sim 5.4 \mu\text{C}/\text{cm}^2$),²⁵ (3-ammoniopyrrolidinium) RbBr_3 ($\sim 3.0 \mu\text{C}/\text{cm}^2$),²⁶ and (3-pyrrolinium) CdCl_3 ($\sim 4.5 \mu\text{C}/\text{cm}^2$).²⁷

All results above indicate that **1** takes a ferroelectric phase transition. Thus, we performed variable-temperature single-crystal XRD analyses to elaborate the origin of ferroelectric phase transition in **1**. As shown in Figure 3a, in ferroelectric phase, the distorted PbBr_6 octahedra make the negatively charged centers evidently orientate along the direction of the *c*-axis. Correspondingly, the positively charged centers of

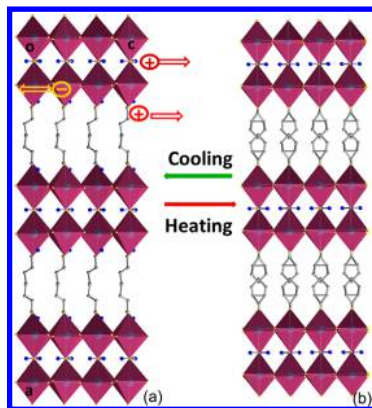


Figure 3. Molecular structures at different temperatures: Perspective view along the *b*-axis at 293 K (a) and 330 K (b).

organic moieties tilt in the opposite direction along the *c*⁺-axis. This separation of positive and negative charge centers results in generation of dipole moments (10.9×10^{-29} C m; Supporting Information) and ferroelectric polarization along the *c*-axis. Different from the polar structure at room temperature, **1** has a centrosymmetric space group of *Cmcm* in paraelectric phase at 330 K. It is evident that the bilayered inorganic framework adopts a highly symmetric configuration, and organic cations become highly disordered (Figure 3b). As a result, the arrangement of all components in **1** meets the requirement of crystallographic symmetry above its *T_c* (i.e., the centrosymmetric space group of *Cmcm*). Hence, thermally induced order-disorder transformation of organic cations and distortion of inorganic moieties synergistically lead to the ferroelectric-to-paraelectric phase transition of **1**.

As elucidated above, the bilayered framework constructed by alternative organic and inorganic components can be considered as quantum well, allowing for rich optical properties originating from free excitation of inorganic layers.²⁸ As shown in Figure 4a, **1** exhibits strong green photoluminescence at 527 nm with narrow emission band. Such single emission peak indicates that the relaxation pathway is dominated by the direct radiative recombination of an exciton.²⁹ Strikingly, **1** displays up-conversion photoluminescence by simultaneous two-photon absorption at room temperature. In order to further study the two-photon absorption effect, film device was prepared by a facile spin-coating at room temperature (Supporting Information, Figure S5). The visible absorbance spectrum shows that **1** has negligible absorbance from wavelength longer than 525 nm (Figure S6). However, when 800 nm laser beam passed through the film of **1**, brightly green emission was observed as displayed in the inset in Figure 4b, indicating that **1** is two-photon active. Such two-photon absorption was further verified by the power-dependent fluorescence intensity (Figure 4c). Figure S7 shows the logarithmic plot of the emission integral versus the pumped power with a slope of around 2, indicating a two-photon absorption mechanism. The photoluminescence process of one-photon (energy larger than the bandgap) and two-photon (energy smaller than the bandgap accompanied a virtual state) light excitation can be deduced (see Figure 4a,b). To quantitatively determine the two-photon absorption, the Z-scan measurement of **1** was carried out. Figure 4d displays the open aperture Z-scan response of the film of **1**. By fitting the nonlinear absorption response curve based on Z-scan theory,³⁰ a giant two-photon absorption coefficient, 5.76×10^3 cm GW⁻¹, is derived for **1**. This value is nearly two-orders of

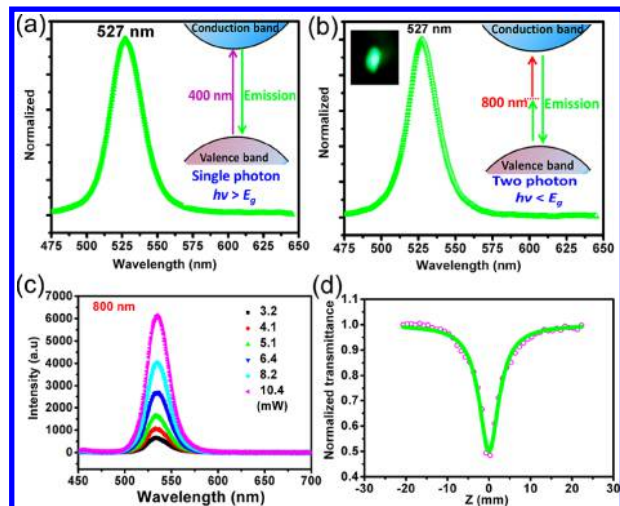


Figure 4. (a) Photoluminescence spectrum of **1** with 400 nm excitation. Inset: schematic diagrams of one-photon absorption and photoluminescence process. (b) Photoluminescence spectrum of **1** under the excitation at 800 nm. Inset: schematic diagrams of two-photon absorption and photoluminescence process (right); strong green emission of **1** excited with 800 nm pulsed laser (left). (c) Excitation intensity-dependent emission spectra of **1** at 800 nm. (d) Open aperture Z-scan responses of **1**.

magnitude larger than those of the notable BaTiO₃ film (51.7 cm GW⁻¹) and Ce:BaTiO₃ (59.3 cm GW⁻¹),⁶ and is comparable to those of CH₃NH₃PbBr₃ film (5.5×10^3 cm GW⁻¹)^{17b} as well as 2D MoS₂ monolayer (7.62×10^3 cm GW⁻¹).³¹ As far as we know, this is the first time to acquire such prominent two-photon absorption in hybrid perovskite ferroelectrics. This finding promises new ferroelectrics for their application in the photonic devices.

In summary, a new hybrid perovskite ferroelectric, (BA)₂(FA)Pb₂Br₇, with prominent two-photon absorption is acquired. It features a quantum-well structure and shows an above-room-temperature ferroelectric phase transition with a notable spontaneous polarization of $3.8 \mu\text{C cm}^{-2}$. Remarkably, it exhibits strong two-photon absorption with a giant absorption coefficient as high as 5.76×10^3 cm GW⁻¹ under the excitation of femtosecond laser. This is the first example of hybrid ferroelectrics with giant two-photon absorption coefficient. These results provide a strategy to design new hybrid perovskite ferroelectrics possessing prominent two-photon absorption for application in photonic devices.

ASSOCIATED CONTENT

Supporting Information

The Supporting Information is available free of charge on the ACS Publications website at DOI: [10.1021/jacs.8b04014](https://doi.org/10.1021/jacs.8b04014).

Crystal data of (BA)₂(FA)Pb₂Br₇, XRD patterns, and additional data (PDF)

X-ray crystallographic data for **1** at 293 K (CIF)

X-ray crystallographic data for **1** at 330 K (CIF)

AUTHOR INFORMATION

Corresponding Authors

*jhluo@fjirsm.ac.cn

*sunzhihua@fjirsm.ac.cn

*xchen@fjirsm.ac.cn

ORCID®

Xueyuan Chen: 0000-0003-0493-839X

Sangen Zhao: 0000-0002-1190-684X

Jun Wang: 0000-0003-0064-3551

Maochun Hong: 0000-0002-1347-6046

Junhua Luo: 0000-0002-7673-7979

Notes

The authors declare no competing financial interest.
 Deposition number CCDC 1589698 and 1589699 for (BA)₂(FA)Pb₂Br₇.

ACKNOWLEDGMENTS

This work was supported by the National Natural Science Foundation of China (21601188, 21622108, 21525104, 21571178, 51502290, and 61675217), Strategic Priority Research Program of the Chinese Academy of Sciences (XDB20000000), and the CAS/SAFEA International Partnership Program for Creative Research Teams. L.L. thanks the supports from Youth Innovation Promotion of CAS (2015240).

REFERENCES

- (1) (a) Scott, J. F.; Paz de Araujo, C. A. *Science* **1989**, *246*, 1400. (b) Garcia, V.; Fusil, S.; Enouz-Vedrenne, K. S.; Mathur, N. D.; Barthelemy, A. *Nature* **2009**, *460*, 7251. (c) Huang, H. *Nat. Photonics* **2010**, *4*, 314. (d) You, Y.-M.; Liao, W.-Q.; Zhao, D.; Ye, H.-Y.; Zhang, Y.; Zhou, Q.; Niu, X.; Wang, J.; Li, P.-F.; Fu, D.-W.; Wang, Z.; Gao, S.; Yang, K.; Liu, J.-M.; Li, J.; Yan, Y.; Xiong, R.-G. *Science* **2017**, *357*, 306.
- (2) Kreisel, J.; Alexe, M.; Thomas, P. A. *Nat. Mater.* **2012**, *11*, 260.
- (3) Grinberg, I.; West, D. V.; Torres, M.; Gou, G.; Stein, D. M.; Wu, L.; Chen, G.; Gallo, E. M.; Akbashev, A. R.; Davies, P. K.; Spanier, J. E.; Rappe, A. M. *Nature* **2013**, *503*, 509.
- (4) (a) Caviglia, A. D.; Scherwitzl, R.; Popovich, P.; Hu, W.; Bromberger, H.; Singla, R.; Mitrano, M.; Hoffmann, M. C.; Kaiser, S.; Zubko, P.; Gariglio, S.; Triscone, J.-M.; Först, M.; Cavalleri, A. *Phys. Rev. Lett.* **2012**, *108*, 13681. (b) Lejman, M.; Vaudel, G.; Infante, I. C.; Gemeiner, P.; Gusev, V. E.; Dkhil, B.; Ruello, P. *Nat. Commun.* **2014**, *5*, 4301.
- (5) Song, J.; Cui, Q.; Li, J.; Xu, J.; Wang, Y.; Xu, L.; Xue, J.; Dong, Y.; Tian, T.; Sun, H.; Zeng, H. *Adv. Opt. Mater.* **2017**, *5*, 1700157.
- (6) Zhang, W. F.; Huang, Y. B.; Zhang, M. S.; Liu, C. L. *Appl. Phys. Lett.* **2000**, *76*, 1003.
- (7) Li, S.; Zhong, X. L.; Cheng, G. H.; Liu, X.; Wang, J. B.; Huang, J.; Song, H. J.; Tan, C. B.; Li, B.; Zhou, Y. C. *Appl. Phys. Lett.* **2014**, *105*, 192901.
- (8) Zhao, Q.; Liu, Y.; Shi, W.; Ren, W.; Zhang, L.; Yao, X. *Appl. Phys. Lett.* **1996**, *69*, 458.
- (9) Zhang, W. F.; Zhang, M. S.; Yin, Z.; Gu, Y. Z.; Du, Z. L.; Yu, B. L. *Appl. Phys. Lett.* **1999**, *75*, 902.
- (10) Zhang, W. F.; Huang, Y. B.; Zhang, M. S. *Appl. Surf. Sci.* **2000**, *158*, 185.
- (11) Shin, H.; Chang, H. J.; Boyd, R. W.; Choi, M. R.; Jo, W. *Opt. Lett.* **2007**, *32*, 2453.
- (12) Liao, W. Q.; Zhang, H.; Hu, Y. C. L.; Mao, J. G.; Ye, H.-Y.; Li, P. F.; Huang, S. D.; Xiong, R.-G. *Nat. Commun.* **2015**, *6*, 7338.
- (13) Ye, H.-Y.; Liao, W.-Q.; Hu, C.-L.; Zhang, Y.; You, Y.-M.; Mao, J.-G.; Li, P.-F.; Xiong, R.-G. *Adv. Mater.* **2016**, *28*, 2579.
- (14) (a) Sun, Z.; Liu, X.; Khan, K.; Ji, C. M.; Asghar, A.; Zhao, S.; Li, L.; Hong, M.; Luo, J. *Angew. Chem., Int. Ed.* **2016**, *55*, 6545. (b) Li, L.; Sun, Z.; Wang, P.; Hu, W.; Wang, S.; Ji, C.; Hong, M.; Luo, J. *Angew. Chem., Int. Ed.* **2017**, *56*, 12150.
- (15) (a) Saparov, B.; Mitzi, D. B. *Chem. Rev.* **2016**, *116*, 4558. (b) Mao, L.; Ke, W.; Pedesseau, L.; Wu, Y.; Katan, C.; Even, J.; Wasielewski, M. R.; Stoumpos, C. C.; Kanatzidis, M. D. *J. Am. Chem. Soc.* **2018**, *140*, 3775.
- (16) (a) Yamada, Y.; Yamada, T.; Phuong, L. Q.; Maruyama, N.; Nishimura, H.; Wakamiya, A.; Murata, Y.; Kanemitsu, Y. *J. Am. Chem. Soc.* **2015**, *137*, 10456. (b) Xu, Y.; Chen, Q.; Zhang, C.; Wang, R.; Wu, H.; Zhang, X.; Xing, G.; Yu, W. W.; Wang, X.; Zhang, Y.; Xiao, M. *J. Am. Chem. Soc.* **2016**, *138*, 3761. (c) Zhang, R.; Fan, J.; Zhang, X.; Yu, H.; Zhang, H.; Mai, Y.; Xu, T.; Wang, J.; Snaith, H. J. *ACS Photonics* **2016**, *3*, 371. (d) Walters, G.; Sutherland, B. R.; Hoogland, S.; Shi, D.; Comin, R.; Sellan, D. P.; Bakr, O. M.; Sargent, E. H. *ACS Nano* **2015**, *9*, 9340. (e) Lu, W.-G.; Chen, C.; Han, D.; Yao, L.; Han, J.; Zhong, H.; Wang, W. *Adv. Opt. Mater.* **2016**, *4*, 1732.
- (17) (a) Takagahara, T.; Hanamura, E. *Phys. Rev. Lett.* **1986**, *56*, 2533. (b) Liu, W.; Xing, J.; Zhao, J.; Wen, X.; Wang, K.; Lu, P.; Xiong, Q. *Adv. Opt. Mater.* **2017**, *5*, 1601045.
- (18) Mitzi, D. B.; Feild, C. A.; Harrison, T. A.; Guloy, A. M. *Nature* **1994**, *369*, 467.
- (19) (a) Tsai, H.; Nie, W.; Blancon, J.-C.; Stoumpos, C. C.; Asadpour, R.; Harutyunyan, B.; Neukirch, A. J.; Verduzco, R.; Crochet, J. J.; Tretiak, S.; Pedesseau, L.; Even, J.; Alam, M. A.; Gupta, G.; Lou, J.; Ajayan, P. M.; Bedzyk, M. J.; Kanatzidis, M. G.; Mohite, A. D. *Nature* **2016**, *536*, 312. (b) Cao, D. H.; Stoumpos, C. C.; Farha, O. K.; Hupp, J. T.; Kanatzidis, M. G. *J. Am. Chem. Soc.* **2015**, *137*, 7843. (c) Xiao, Z.; Kerner, R. A.; Zhao, L.; Tran, N. L.; Lee, K.-M.; Koh, T.-W.; Scholes, G. D.; Rand, B. P. *Nat. Photonics* **2017**, *11*.10810.1038/nphoton.2016.269
- (20) (a) Lee, C.-H.; Orloff, N. D.; Birol, T.; Zhu, Y.; Goian, V.; Rocas, E.; Haislmaier, R.; Vlahos, E.; Mundt, J. A.; Kourkoutis, L. F.; Nie, Y.; Biegalski, M. D.; Zhang, J.; Bernhagen, M.; Benedek, N. A.; Kim, Y.; Brock, J. D.; Uecker, R.; Xi, X. X.; Gopalan, V.; Nuzhnyy, D.; Kamba, S.; Muller, D. A.; Takeuchi, I.; Booth, J. C.; Fennie, C. J.; Schloss, D. G. *Nature* **2013**, *502*, 532. (b) Strayer, M. E.; Gupta, A. S.; Akamatsu, H.; Lei, S.; Benedek, N. A.; Gopalan, V.; Mallouk, T. E. *Adv. Funct. Mater.* **2016**, *26*, 1930.
- (21) Cai, H.-L.; Zhang, W.; Ge, J.-Z.; Zhang, Y.; Awaga, K.; Nakamura, T.; Xiong, R.-G. *Phys. Rev. Lett.* **2011**, *107*, 147601.
- (22) Fukunaga, M.; Noda, Y. *J. Phys. Soc. Jpn.* **2008**, *77*, 064706.
- (23) Gesi, K. *J. J. Phys. Soc. Jpn.* **1990**, *59*, 432.
- (24) Zhang, Y.; Ye, H.-Y.; Zhang, W.; Xiong, R.-G. *Inorg. Chem. Front.* **2014**, *1*, 118.
- (25) Zhang, Y.; Liao, W.-Q.; Fu, D.-W.; Ye, H.-Y.; Chen, Z.-N.; Xiong, R.-G. *J. Am. Chem. Soc.* **2015**, *137*, 4928.
- (26) Pan, Q.; Liu, Z.-B.; Tang, Y.-Y.; Li, P.-F.; Ma, R.-W.; Wei, R.-Y.; Zhang, Y.; You, Y.-M.; Ye, H.-Y.; Xiong, R.-G. *J. Am. Chem. Soc.* **2017**, *139*, 3954.
- (27) Ye, H.-Y.; Zhang, Y.; Fu, D.-W.; Xiong, R.-G. *Angew. Chem., Int. Ed.* **2014**, *53*, 11242.
- (28) (a) Blancon, J.-C.; Tsai, H.; Nie, W.; Stoumpos, C. C.; Pedesseau, L.; Katan, C.; Kepenekian, M.; Soe, C. M. M.; Appavoo, K.; Sfeir, M. Y.; Tretiak, S.; Ajayan, P. M.; Kanatzidis, M. G.; Even, J.; Crochet, J. J.; Mohite, A. D. *Science* **2017**, *355*, 1288. (b) Dou, L. T.; Wong, A. B.; Yu, Y.; Lai, M. L.; Kornienko, N.; Eaton, S. W.; Fu, A.; Bischak, C. G.; Ma, J.; Ding, T. N.; Ginsberg, N. S.; Wang, L. W.; Alivisatos, A. P.; Yang, P. D. *Science* **2015**, *349*, 1518.
- (29) Muljarov, E. A.; Tikhodeev, S. G.; Gippius, N. A.; Ishihara, T. *Phys. Rev. B: Condens. Matter Mater. Phys.* **1995**, *51*, 14370.
- (30) Van Stryland, E. W.; Vanherzeele, H.; Woodall, M. A.; Soileau, M. J.; Smirl, A. L.; Guha, S.; Boggess, T. F. *Opt. Eng.* **1985**, *24*, 613.
- (31) Li, Y.; Dong, N.; Zhang, S.; Zhang, X.; Feng, Y.; Wang, K.; Zhang, L.; Wang, J. *Laser Photonics. Rev.* **2015**, *9*, 427.